Charge Carrier Diffusion and Recombination near Misfit Dislocations in GaAsP/GaInP Heterostructures

T.H. Gfroerer,[1] A. Edmondson,[1] Lilian Korir,[1] Fan Zhang,[2] Yong Zhang,[2] and M.W. Wanlass[3]

[1] *Davidson College, Davidson, NC USA*
[2] *Univesity of North Carolina at Charlotte, Charlotte, NC USA*
[3] *Wanlass Consulting, Norwood, CO USA*

***Abstract*—GaAsP alloys are good candidates for the upper junction in Si-based dual-junction tandem solar cells. However, monolithic growth of GaAsP on Si is limited by dislocation formation due to lattice mismatch. When metamorphic GaAsP is grown on GaAs substrates, dark crosshatch features can be observed in spatially-resolved electroluminescence and photoluminescence measurements. These features can be attributed to misfit dislocations in the epitaxial layers. We compare photoluminescence imaging with complementary confocal mapping measurements to test models of diffusion and recombination near misfit dislocations in a GaAsP/GaInP heterostructure. The crosshatch features become sharper with increased photoexcitation in accordance with reduced lifetimes and diffusion distances. However, the imaging and mapping experiments require different defect-related recombination rates in our computational models.**

Keywords—electroluminescence, photoluminescence, imaging, confocal mapping, misfit dislocations, diffusion, recombination

I. Introduction

Silicon-based photovoltaic technology continues to dominate the solar cell market, but the efficiency of single-junction silicon devices is ultimately limited by poor conversion of high energy light. Future improvements in Silicon-based devices are likely to rely on the addition of one or more higher energy junctions to improve the conversion efficiency of light in the visible range of the solar spectrum. The top material candidates for these new junctions include III-V alloys and perovskites. [1] Within the family of III-Vs, GaAsP, [2] GaInP, and AlGaAs [3] are suitable alloys for achieving the 1.7 eV bandgap required for optimal Si-based dual-junction performance.

In this contribution, we report on photoluminescence (PL) imaging and PL confocal mapping of a 1.67 eV GaAsP/GaInP double heterostructure grown on a GaAs substrate. In both measurements, dark crosshatch features are observed in the plan-view luminescence emission pattern from the structure, which we attribute to dangling bonds and defect states associated with misfit dislocations. [4] We study how these features change with photoexcitation in both experiments and model the behavior with simple steady-state rate equation algorithms. While the preliminary simulations can reproduce the changing profiles that result from variation in carrier lifetime, different defect-related recombination parameters are required to fit the results of the two experiments.

II. Experiment

The GaAsP/GaInP double heterostructure (DH) incorporates 3 GaAsP step-grading layers between the GaAs substrate and the DH to accommodate approximately 0.5% lattice mismatch. The nominally lattice-matched DH is not intentionally doped and has a 2 μm $GaAs_{0.8}P_{0.2}$ active layer, with a room-temperature (RT) PL peak emission of approximately 1.67 eV.

For PL imaging, the sample is illuminated with an unfocused 532 nm laser having an approximate spot size of 5.2×10^{-3} cm^2. PL and EL images are obtained with a cooled Q-Imaging Rolera XR CCD camera, which has extended infrared sensitivity to 1μm. Two OG 570 long-pass filters are used to eliminate scattered laser light. The camera is fitted with an Edmund Scientific VZM 300 imaging lens set to 3X magnification, yielding image pixel dimensions of 4.4×4.4 μm^2.

PL mapping experiments are conducted at RT with a Horiba LabRAM HR confocal Raman microscope. In this system, a 532 nm laser is focused by a 50X long working distance lens to a spot with a diameter of approximately 2 μm. Neutral density filters in the laser path are used to control the incident optical power, which equals 114 μW unfiltered. The confocal geometry of the instrument ensures that the PL sample volume coincides with the photoexcitation volume. The PL spectrum is acquired via a CCD detector in a 24 nm window centered on the peak emission (726 – 750 nm). PL maps are obtained by laterally translating the sample under the objective with a precise, motorized stage.

III. Results

Representative RT PL images and confocal maps of a prominent crosshatch feature are shown in Fig. 1, with the images on the left and the maps on the right. The upper results were obtained at low laser power and the lower results were obtained at high laser power. The dark spots and lines mark defective regions where non-radiative recombination dominates, carriers are depleted, and PL emission is reduced. In particular, we attribute the isolated spots to threading dislocations and the lines to more extended misfit dislocations. In both experiments, we see clear changes in the extent of defective regions (driven by changes in the diffusion of electrons and holes) when the laser power is increased. [5] Brighter illumination produces higher steady-state carrier densities and recombination rates, along with reduced lifetimes and diffusion lengths. Hence, defective features appear sharper at high excitation.

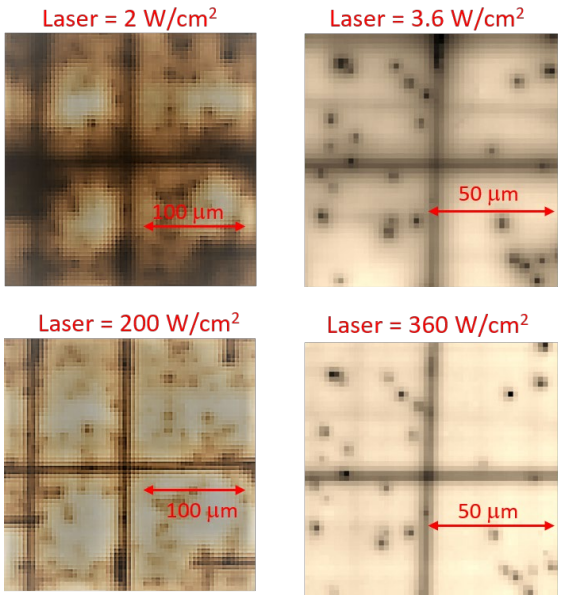

Fig. 1. Representative RT PL images and maps of a crosshatch feature in the emission pattern from the GaAsP/GaInP DH. PL images are on the left and confocal maps are on the right with lower excitation above and higher excitation below.

IV. ANALYSIS

We start by selecting a portion of the horizontal line having relatively few adjacent features above and below the line and then averaging the columns of pixels in this region. This procedure yields a line profile of the PL intensity across the horizontal line. We divide the PL count in each pixel by the integration time to obtain a relative measure of the radiative recombination rate in each pixel.

The local densities of electrons (n) and holes (p) in a given pixel are assumed to be equivalent ($n = p$) and independent of time in steady-state:

$$\frac{dn}{dt} = G + J - Bn^2 - A_P n = 0 \qquad (1)$$

where G is the electron-hole pair generation rate, J is the net diffusive flux into the pixel, Bn^2 is the radiative recombination rate, and $A_P n$ is the nonradiative recombination rate due to uniformly-distributed point defects. An additional nonradiative loss mechanism $A_L n$ is included in the rate equation for the pixel at the center of the line defect. For the imaging experiment, G is the same in every pixel, but in the mapping experiment, G is zero everywhere except the photoexcited pixel. We compute the diffusive flux using the carrier density in adjacent pixels:

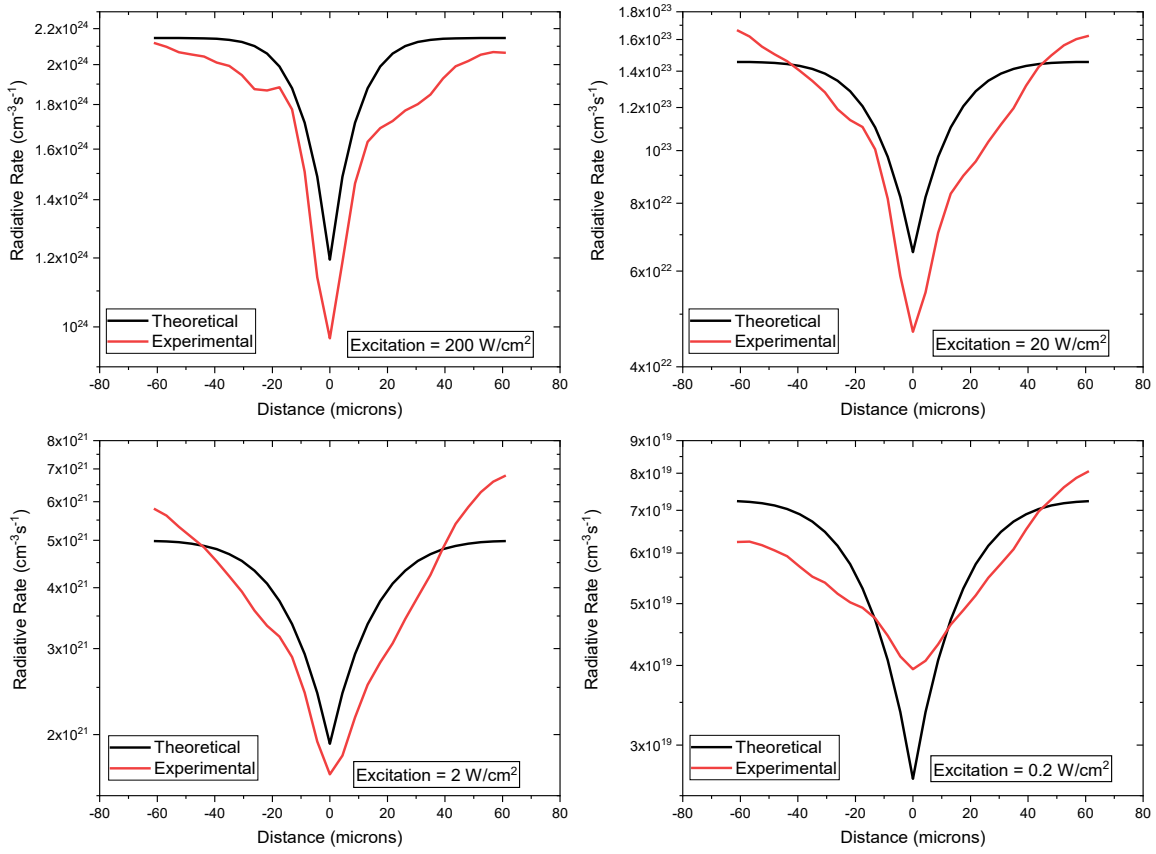

Fig. 2: PL imaging line profiles of the horizontal line defect under different photoexcitation conditions, showing how the radiative emission varies with distance from the misfit dislocation.

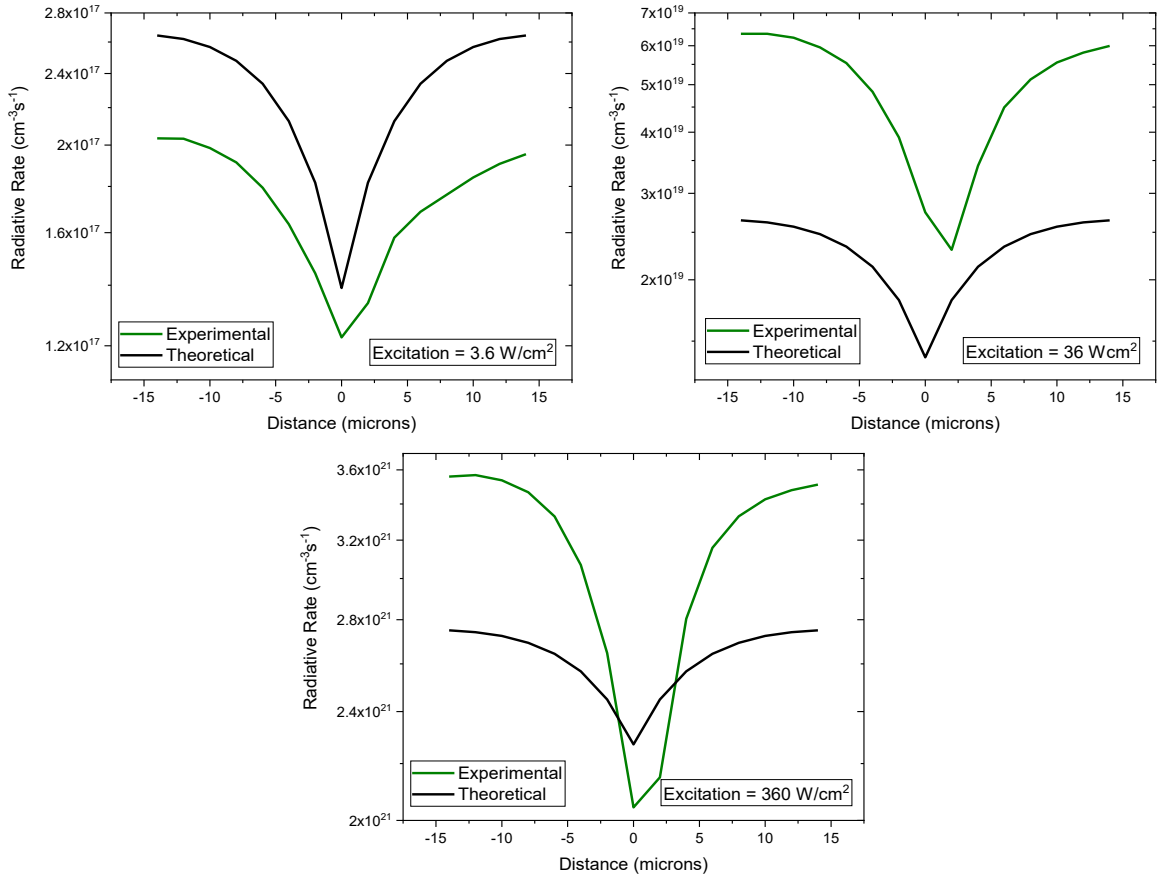

Fig. 3: PL confocal mapping line profiles of the horizontal line defect under different photoexcitation conditions.

$$J = D\left(n_{left} + n_{right} - 2n\right)/w^2 \qquad (2)$$

where D is the diffusivity and w is the width of the pixel. Using periodic boundary conditions, we iterate this calculation until a steady-state density distribution across the line defect is achieved. Then the theoretical radiative rate Bn^2 is divided by a loss factor LF, which accounts for light extraction efficiency and system response, and compared with the measured PL signal in each pixel. A basin-hopping algorithm [6] is used to identify the fitting parameters LF, A_P, and A_L that yield the minimum error between the experimental and simulated results. Fig. 2 shows the simulation results for the imaging experiment and Fig. 3 shows the results for the confocal mapping experiment. The optimized parameters are given in Table I.

TABLE I. COMPUTATIONAL FITTING PARAMETERS

	Experiment	
Parameter	***Imaging***	***Mapping***
B	2×10^{-10} cm^{3}s^{-1}	
D	1×10^2 cm^2 s^{-1}	
LF	2700	0.51
A_P	4.2×10^6 s^{-1}	1.2×10^8 s^{-1}
A_L	1.4×10^8 s^{-1}	4.5×10^8 s^{-1}

The density profiles for mapping are narrower as predicted by theory, [7] corroborating the diffusion algorithms. And the nonradiative recombination coefficients at the site of the line defect are generally consistent because the area of the defective pixel in the mapping experiment is approximately 4 times smaller and requires a proportionally higher rate. However, the discrepancy between the coefficients for nonradiative recombination at point defects points to limitations of the ABC recombination model [8] and suggests that different defect-related mechanisms are operating under the conditions probed by the two experiments. While the photoexcitation densities are comparable, diffusion out of the highly localized excitation volume in the mapping experiment yields steady-state carrier densities that are approximately two orders of magnitude smaller. The equivalent density assumption ($n = p$) is least accurate at low densities and prior work on GaAs/GaInP [5] has demonstrated that defect-related recombination can be strongly augmented in this extremely low-density regime.

Finally, we note that these plan-view measurements probe a fixed depth in the structure and cannot identify inclined misfits where the depth of the defective region may vary with lateral position. A multi-dimensional approach would provide a more complete picture of the misfit dislocation network in this system.

ACKNOWLEDGMENT

The work at the UNCC was supported by ARO/Electronics (Grant No. W911NF-16-1-0263).

REFERENCES

[1] Martin A. Green, Ewan D. Dunlop, Jochen Hohl‐Ebinger, Masahiro Yoshita, Nikos Kopidakis, and Anita W.Y. Ho‐Baillie, "Solar cell efficiency tables (Ver. 55)," *Prog. Photovoltaics* 28, pp. 3–15, 2020.

[2] Tyler J. Grassman *et al*., "Toward >25% efficient monolithic epitaxial GaAsP/Si tandem solar cells," *Proc. 46th IEEE Photovoltaic Specialists Conference*, 2019.

[3] Ahmed Ben Slimane *et al*., "AlGaAs/InGaP MBE-grown heterostructures for 1.73eV solar cells with 18.7% efficiency," *Proc. 46th IEEE Photovoltaic Specialists Conference*, 2019.

[4] T. H. Gfroerer, M. J. Romero, M. M. Al-Jassim, and M. W. Wanlass, "Band-to-band and sub-band gap cathodoluminescence from GaAsP/GaInP epistructures grown on GaAs substrates," *J. Lumin.* 122–123, pp. 348–351 (2007).

[5] T. H. Gfroerer, Yong Zhang, and M. W. Wanlass, "An extended defect as a sensor for free carrier diffusion in a semiconductor," *Appl. Phys. Lett.* 102 (1), 012114 (2013).

[6] https://docs.scipy.org/doc/scipy/reference/generated/scipy.optimize.basinhopping.html

[7] Fengxiang Chen, Yong Zhang, T.H. Gfroerer, A.N. Finger, and M.W. Wanlass, "Spatial resolution versus data acquisition efficiency in mapping an inhomogeneous system with species diffusion," *Sci. Rep.* 5, 10542 (2015).

[8] Fan Zhang, Jose F. Castaneda, Timothy H. Gfroerer, Daniel Friedman, Yong-Hang Zhang, Mark W. Wanlass and Yong Zhang, "An all optical approach for comprehensive in-operando analysis of radiative and nonradiative recombination processes in GaAs double heterostructures," *Light Sci. Appl.* 11, 137 (2022)